Physiological Fluid Dynamics*

O. E. Jensen

Centre for Mathematical Medicine, School of Mathematical Sciences,
University of Nottingam, University Park, Nottingham NG7 2RD, UK
`Oliver.Jensen@nottingham.ac.uk`

June 30, 2003

Contents

---

*Summer School Program — Introduction to Mathematical Medicine, University of Waterloo. ©Oliver E. Jensen

1   Introduction

1.1   Physiological flows

While microscopic organisms can often rely on molecular diffusion to provide them with nutrients and to remove waste products, large organisms require more efficient means of transporting materials within their bodies. This is accomplished using flowing liquids and gases. For example, as we breathe in, oxygen is swept into the lungs through a network of airways. It diffuses into blood across the walls of alveoli and is then pumped by the heart through an extensive network of blood vessels to all parts of the body. Blood then collects the waste products of metabolism and efficiently eliminates them: carbon dioxide is carried back to the lungs, from where it is exhaled; urea is converted into another liquid (urine) in the kidneys, from where it is actively pumped to the bladder. The extraction and transport of nutrients obtained from food also exploits flow. Semi-solid food is actively swept down the oesophagus to the stomach and intestines, from where key nutrients are extracted and carried by blood to supply cells throughout the body. The elimination of waste food from the gut again requires active (peristaltic) pumping, albeit of material with complex rheological (flow) properties.

Fluids in the body are used not only for transport. They can also provide a protective film on surfaces exposed to the outside world. The front of the eye (the cornea) is coated with a thin tear film; this coating is refreshed every time we blink. Our airways are wet: the nose and mouth are coated with mucus and saliva respectively, and lung airways are coated with a layer of mucus, which traps inhaled particles that are then swept moutwards by beating cilia (small hairs) on airway epithelial cells, allowing the particles to be removed by coughing or swallowing. In certain diseases, the liquid lining of lung airways can block airways and make breathing difficult. Fluids are also involved in lubricating the sliding or squeezing motions of adjacent surfaces (for example in joints and in the pleura surrounding the lung) and in sensory organs (the aqueous humor in the eye is a viscous liquid; liquid inertia is exploited in the cochlea in the ear in hearing and in balance).

Physiological fluid dynamics involves the study of idealised model problems (either experimental or theoretical) that characterise the key features of flows in the body. The understanding we gain from models improves both our knowledge of basic physiology and pathology, and can also be exploited in engineering new clinical therapies and biomedical devices. The key features that distinguish physiological flows from other branches of fluid mechanics include the following.

- **Pulsatility.** Flows in arteries, for example, are strongly pulsatile due to the beating of the heart. Airflow in the lung is also pulsatile during breathing. This unsteadiness must be investigated often within highly *complex geometries.*

- **Deformability.** The vessels in the body that transport blood, air, urine or food are all elastic to some degree. Flow-induced forces can deform the walls of the vessels, and these deformations can in turn affect the flow. *Flow-structure interactions* are important across a wide range of scales, from the deformation of individual blood cells squeezing through narrow capillaries, to flow-induced instabilities of airways leading to wheezing on expiration or to the motion of heart valves during the pumping of the heart.

- **Activity.** Biological structures are not always mechanically passive. Vessels with muscular linings respond to the forces acting on them and can actively generate flows. Thus smooth muscle lining the walls of airways constricts during an asthma attack, small ateries constrict in the regulation of blood pressure, and the walls of the oesophagus and ureter generate coordinated movements to propel their contents via *peristalsis.*

- **Remodeling.** A vessel may also respond to imposed fluid forces over longer timescales. The endothelial cells lining a blood vessel, for example, convert fluid-mechanical forces into a biological response by altering gene expression and hence the biological function of the cell. This is demonstrated dramatically by the reorientation within hours of cultured endothelial cells exposed to flow. This long-term adaption may be beneficial or harmful. Low and oscillatory *wall shear stresses* (see below) in blood vessels, for example, are correlated with the onset of atherosclerosis, a disease in which fatty deposits are laid down in the wall of blood vessels. Over long times, these deposits can grow to occlude the vessel. If this happens in coronary arteries, heart muscle is starved of oxygen, which leads to angina or a heart attack. An understanding of the effects of vessel geometry on flow has been of major significance in approaching this disease.

In these lectures we will examine a few simple models of flows that characterise some of these effects. A theme linking many of these models is the use of asymptotic long-wave (thin-film or boundary-layer) approximations to simplify the governing equations, and to provide tractable models that capture the important physics.

Good surverys of large areas of physiological fluid dynamics are provided by Lighthill (1975), McDonald (1974) and Pedley (1980, 2000).

1.2 Fundamentals of internal flows

We start with a crash course in basic fluid mechanics.

To a good approximation, biological fluids have constant density ρ. This means that any velocity field

$$\mathbf{u}^*(\mathbf{x}^*, t^*) = (u^*(\mathbf{x}^*, t^*), v^*(\mathbf{x}^*, t^*), w^*(\mathbf{x}^*, t^*))$$

defined with respect to Cartesian co-ordinates $\mathbf{x}^* = (x^*, y^*, z^*)$, telling us the velocity of the fluid particle at position $\mathbf{x}^*$ and time t^*, satisfies the *incompressibility* condition

$$\nabla^* \cdot \mathbf{u}^* = 0, \quad \text{i.e.} \quad u_{x^*}^* + v_{y^*}^* + w_{z^*}^* = 0, \tag{1.1}$$

where subscripts denote partial derivatives. This condition ensures that a small blob of fluid has fixed volume as it is swept along and deformed by a flow.

Newton's second law ('F=ma') for a fluid particle is written

$$\rho \frac{\mathrm{D}\mathbf{u}^*}{\mathrm{D}t^*} = \nabla^* \cdot \boldsymbol{\sigma}^* \tag{1.2}$$

where

$$\frac{\mathrm{D}\mathbf{u}^*}{\mathrm{D}t^*} \equiv \mathbf{u}_{t^*}^* + (\mathbf{u}^* \cdot \nabla^*)\mathbf{u}^* \tag{1.3}$$

is the *material derivative* (a time derivative following a moving fluid particle). Even in a *steady* flow ($\mathbf{u}_{t^*}^* = 0$) a fluid particle can be accelerated if it is swept into a region of faster-moving flow ($|(\mathbf{u}^* \cdot \nabla^*)\mathbf{u}^*| > 0$). $\boldsymbol{\sigma}^\star$ is the *stress tensor*, defined such that the force per unit area on a surface with unit normal $\mathbf{n}$ is $\boldsymbol{\sigma}^* \cdot \mathbf{n}$; equivalently, the force per unit volume acting on an element of fluid is $\nabla^* \cdot \boldsymbol{\sigma}^*$. We must relate the stress $\boldsymbol{\sigma}^*$ to the *rate of strain* of the fluid (the rate at which fluid particles are distorted by the flow). For *Newtonian* fluids, this relation is linear, and is expressed as

$$\boldsymbol{\sigma}^* = -p^\star \mathbf{I} + \mu(\nabla^\star \mathbf{u}^\star + \nabla^\star \mathbf{u}^{\star T})$$

such that (1.2) becomes

$$\rho \frac{\mathrm{D}\mathbf{u}^*}{\mathrm{D}t^*} = -\nabla^* p^* + \mu \nabla^{*2} \mathbf{u}^*, \tag{1.4}$$

where $p^*(\mathbf{x}^*, t^*)$ is the *pressure* in the fluid and μ is its viscosity, assumed constant. Water and air are Newtonian to a good approximation; water has viscosity $\mu \approx 0.01$ gm/cm s. Sometimes we write $\mu = \rho\nu$, where the *kinematic viscosity* ν has dimensions length^2/time.

We need to introduce pressure in (1.4) in order to satisfy the incompressibility condition (1.1). A fluid particle in a pressure gradient $\nabla^* p^*$ will experience a higher pressure on one side than the other, and thus experiences a force from high to low pressure. The viscous term $\mu \nabla^{*2} \mathbf{u}^*$ represents the effects of friction on a fluid particle; it acts to suppress velocity gradients (or *shear*).

Biological fluids are complex materials. They may be a concentrated suspension of deformable cells (such as blood) or a semi-solid gel (such mucus or food). Such materials typically have a nonlinear stress/rate-of-strain relation, and they may also be *viscoelastic*, i.e. having elastic (solid-like) as well as purely viscous properties. Such behavior is called *non-Newtonian*, and gives rise to equations of motion more complex than (1.4). Here we will restrict attention to Newtonian viscous liquids governed by (1.4). Blood in large blood vessels may be reasonably accurately approximated as a Newtonian liquid with viscosity roughly four times that of water. For vessels of diameter below about 500 μm, however (so that the vessel diameter is roughly comparable to the 8-μm-diameter of a red blood cell), blood has more complex rheological behavior.

The *Navier–Stokes equations* (1.1, 1.4) are the starting point for our models. They must be supplemented with appropriate boundary conditions. At a stationary rigid surface S, for example, fluid can neither flow through the surface (asssuming it is impermeable) nor parallel to it (because viscous fluids stick to surfaces), implying

$$\mathbf{u}^* = \mathbf{0} \quad \text{on} \quad S. \tag{1.5}$$

We will discuss other boundary conditions as appropriate below.

In many problems, it is helpful to *non-dimensionalise* the governing equations. For example, if we consider flow in a tube of radius a, with some average axial speed U_0, that may be forced at a frequency ω, we write

$$\mathbf{x}^* = a\mathbf{x}, \quad t^* = t/\omega, \quad \mathbf{u}^* = U_0 \mathbf{u}(\mathbf{x}, t), \quad p^* = (\mu U_0/a) p(\mathbf{x}, t). \tag{1.6}$$

Equations (1.1, 1.4) then become

$$\nabla \cdot \mathbf{u} = 0, \quad \alpha^2 \mathbf{u}_t + Re(\mathbf{u} \cdot \nabla)\mathbf{u} = -\nabla p + \nabla^2 \mathbf{u}, \tag{1.7}$$

where

$$Re = \frac{\rho U_0 a}{\mu}, \quad \alpha = \left(\frac{\rho a^2 \omega}{\mu}\right)^{1/2}$$

are the *Reynolds number* and *Womersley number* respectively. Each dimensionless parameter characterises the relative importance of inertial to viscous forces. When $Re \ll 1$, $\alpha \ll 1$, we have slow, *creeping* or *Stokes* flow, which is dominated by viscosity and is always smooth and *laminar*. Such flows arise in the smallest capillaries or in the smallest airways of the lung. For $Re \gg 1$ or $\alpha \gg 1$, flow is rapid and is dominated by inertia, and can often become unstable and even *turbulent* (for steady pipe flow, turbulence arises for $Re > 2000$ approximately). In large arteries, $30 < Re < 2000$ and $\alpha > 1$ ($\alpha \approx 15-20$ in the aorta). Transition to turbulence can therefore occur in the largest arteries during peak flows, and certainly occurs during expiratory airflow in the lungs, particularly under extreme conditions such as coughing or sneezing.

1.3 Unidirectional flows

Accurately describing most flows for which $Re \gg 1$ challenges today's most powerful computers. We will therefore consider only some special cases. Consider for example the *unidirectional* flow $\mathbf{u} = w\hat{\mathbf{z}}$
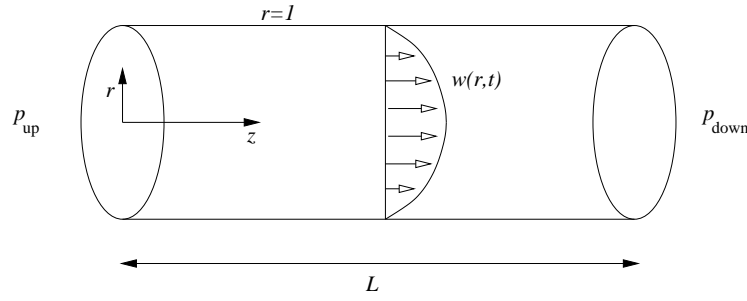
Figure 1: Unidirectional flow in a tube.

in a uniform cylindrical tube (a model for a blood vessel), where $\hat{\mathbf{z}}$ is the unit vector pointing along the axis of the tube (Fig. 1). Equation (1.1) demands that $w_z = 0$, so that $w = w(x, y, t)$. (Here subscripts x, y, z, t etc. denote derivatives.) It follows that $(\mathbf{u} \cdot \nabla)\mathbf{u} = ww_z\hat{\mathbf{z}} = \mathbf{0}$, so the awkward nonlinear term in (1.7) vanishes. Equation (1.7b) reduces to the following three scalar equations:

$$p_x = 0, \quad p_y = 0, \quad \alpha^2 w_t = -p_z + w_{xx} + w_{yy}. \tag{1.8}$$

Thus $p = p(z, t)$; furthermore, because p_z is balanced by terms that are independent of z, p_z must be a function of t alone. Thus $w(x, y, t)$ satisfies a diffusion equation, forced by an imposed (possibly time-dependent) pressure gradient.

We can simplify (1.8) further by assuming the flow is *axisymmetric*, i.e. $w = w(r, t)$ where $r = (x^2 + y^2)^{1/2}$ is the polar radial coordinate in the (x, y)-plane. Then

$$\alpha^2 w_t = -p_z + \frac{(rw_r)_r}{r}. \tag{1.9}$$

The factors of r arise from the representation of ∇^2 in cylindrical polar coordinates. A further assumption is to suppose p_z and w are *steady*, so that $w_t = 0$. Suppose that the dimensional pressure gradient $p_{z*}^* = -G$, say, for some constant $G = (p_{up} - p_{down})/L$, assuming pressures p_{up} and p_{down} are applied along a length L of tube (Fig. 1). We may then set $U_0 = a^2 G/\mu$ in (1.6), so that $p_z = -1$. We can then integrate

$$0 = 1 + \frac{1}{r}(rw_r)_r$$

to give

$$w_r = -\frac{r}{2} + \frac{A}{r}$$

for some constant A. Because w must be bounded at the centre of the tube ($r = 0$) we must have $A = 0$. Integrating again and imposing the *no-slip condition* (1.5) at the tube wall ($w = 0$ on $r = 1$) we obtain

$$w = \tfrac{1}{4}(1 - r^2). \tag{1.10}$$

In our original dimensional units, (1.10) is

$$w^* = -\frac{G}{4\mu}(a^2 - r^{*2}), \qquad G = \frac{p_{up} - p_{down}}{L}.$$

This is *Poiseuille* flow, which has a parabolic *velocity profile* across the tube. This fundamental flow was first described by the physician Jean Poiseuille (1797-1869) in his investigations of blood flow.

The dimensional *volume flux*, i.e. the volume of fluid passing a fixed z-location per unit time, is

$$Q^* = \int_{r^* \leq a} w^* \, \mathrm{d}S = a^2 U_0 \int_0^1 2\pi r w \, \mathrm{d}r = \frac{\pi a^4 G}{8\mu}. \tag{1.11}$$

Because the flux is proportional to a^4, large pressure gradients are necessary to force viscous fluid through very narrow blood vessels. (The biggest pressure drop in the systemic circulation therefore occurs across the capillaries.) The ratio $G/Q^* = 8\mu/\pi a^4$ is called the *viscous resistance*, and

$$\overline{w^\star} = \frac{1}{\pi a^2} \int w^\star \, \mathrm{d}S = \frac{Q^*}{\pi a^2} = \frac{a^2 G}{8\mu} \tag{1.12}$$

is the *cross-sectionally-averaged flow speed*. For a flow driven by a fixed volume flux, $\overline{w^\star}$ increases where a decreases; for a flow driven by a fixed pressure gradient, however, $\overline{w^\star}$ decreases where a decreases. A further important quantity is the *wall shear stress*, which is the viscous force per unit area exerted by the flow on the wall of the vessel (the quantity $-\hat{\mathbf{z}} \cdot \boldsymbol{\sigma} \cdot \hat{\mathbf{r}}$). For Poiseuille flow, this is

$$\tau = -\mu w_{r^*}^* \big|_{r^*=a} = -\frac{\mu U_0}{a} w_r \big|_{r=1} = \frac{aG}{2} = \frac{4\mu Q^*}{\pi a^3}. \tag{1.13}$$

At a bifurcation, where a parent blood vessel (of radius a, carrying flux Q) splits into daughter vessels (with radii a_1 and a_2 carrying fluxes Q_1 and Q_2), mass conservation requires that $Q = Q_1 + Q_2$. The *uniform shear hypothesis* proposes that τ is the same in parent and daughter vessels. Assuming blood flow is a Poiseuille flow (which is debatable —see below), (1.13) requires

$$a^3 = a_1^3 + a_2^3. \tag{1.14}$$

Observations support this prediction; (1.14) is known as *Murray's law*.

1.4   Oscillatory flow in a tube

We now relax our assumption of steadiness and ask instead how flow in a uniform tube responds to an oscillatory pressure gradient with zero mean

$$p_{z^*}^* = -G \cos(\omega t^*),$$

where ω is a constant frequency. In dimensionless terms, (1.9) becomes

$$\alpha^2 w_t = \cos t + \frac{1}{r} (r w_r)_r. \tag{1.15}$$

Again, the boundary conditions are $w(1, t) = 0$, $w_r(0, t) = 0$, implying no-slip on the tube wall, and smooth bounded solutions at $r = 0$. We seek periodic solutions of the form

$$w = \Re \left[g(r) e^{it} \right],$$

for some complex function $g(r)$, where $\Re$ denotes 'real part.' Substituting into (1.15) we have

$$i\alpha^2 g - \frac{1}{r} (r g_r)_r = 1, \quad \text{where} \quad g(1) = 0, \quad g_r(0) = 0. \tag{1.16a}$$

Setting $g(r) = 1/(i\alpha^2) + \hat{g}(\hat{r})$, where $\hat{r} = \alpha e^{-i\pi/4} r$, gives $\hat{g}_{\hat{r}\hat{r}} + \hat{g}_{\hat{r}}/\hat{r} + \hat{g} = 0$, one of Bessel's equations, from which we find

$$g(r) = \frac{1}{i\alpha^2} \left(1 - \frac{J_0(\alpha e^{-i\pi/4} r)}{J_0(\alpha e^{-i\pi/4})} \right). \tag{1.17}$$
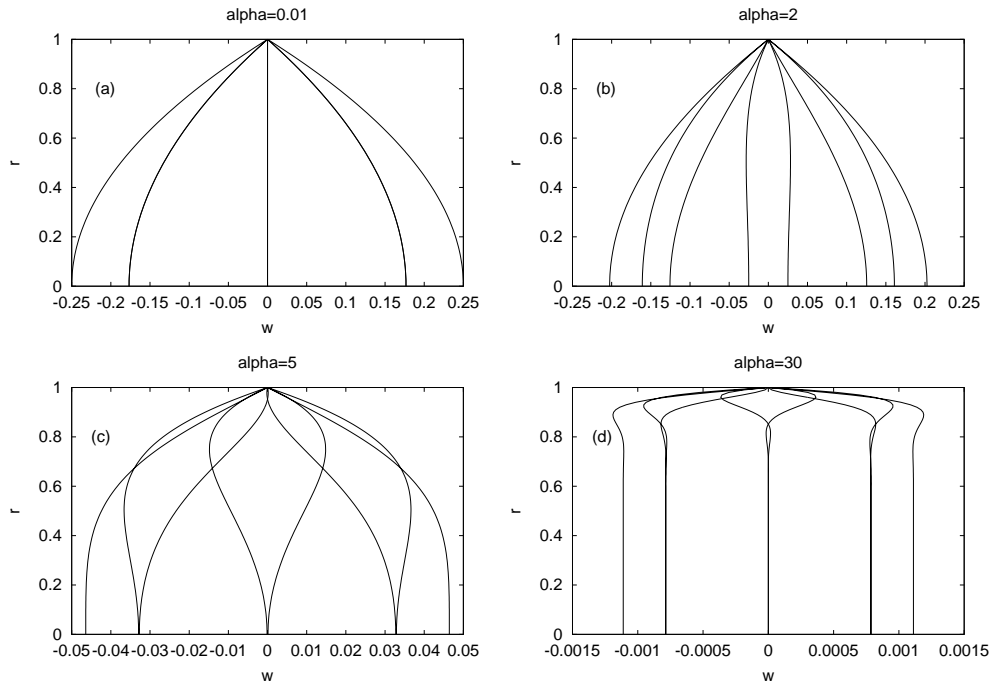
Figure 2: $w(r)$ (see 1.18) for $\alpha = 0.01$, 2, 5 and 30, at $t = 0, \pi/4, \pi/2, 3\pi/4, ..., 7\pi/4$.

Here J_0 is Bessel's function of order zero (i.e. $z^2 J_{0zz} + z J_{0z} + z^2 J_0 = 0$, $J_{0z}(0) = 0$). Thus

$$w = \frac{1}{\alpha^2} \Re \left[\left(1 - \frac{J_0(\alpha e^{-i\pi/4} r)}{J_0(\alpha e^{-i\pi/4})} \right) e^{i(t-\pi/2)} \right]. \tag{1.18}$$

In the original dimensional variables, (1.18) becomes

$$w^* = \frac{G}{\rho\omega} \Re \left[\left(1 - \frac{J_0(\alpha e^{-i\pi/4} r^*/a)}{J_0(\alpha e^{-i\pi/4})} \right) e^{i(\omega t^* - \pi/2)} \right].$$

Examples of w are shown in Fig. 2. At low α the flow has a parabolic profile: we may understand this by using $J_0(z) \approx 1 - (z^2/4) + O(z^4)$ as $z \to 0$, from which one finds that

$$w \approx \left(\frac{1 - r^2}{4} \right) \cos t \qquad (\alpha \ll 1).$$

The flow is a *quasi-steady* Poiseuille flow, in phase with the forcing due to the pressure gradient.

At high α, w is uniform in the core of the tube, and varies rapidly near the walls. Using the identity

$$J_0(z) \approx \sqrt{\frac{2}{\pi z}} \cos \left(z - \tfrac{1}{4}\pi \right) \qquad z \to \infty$$

with $|\arg(z)| < \pi$, it follows that

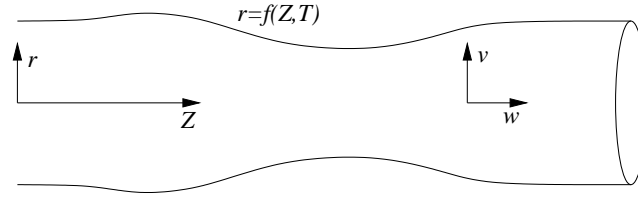$$g(r) \approx \frac{1}{i\alpha^2} \left[1 - \exp \left(-\frac{(1+i)}{\sqrt{2}} \alpha(1 - r) \right) \right].$$

Figure 3: Almost unidirectional flow in a non-uniform tube

Thus unless r is very close to 1, the exponential term is vanishingly small as $\alpha \to \infty$, so that in the core of the tube, $g \approx 1/i\alpha^2$, so that here w in (1.18) is

$$w \approx \Re\left[\frac{e^{it}}{i\alpha^2}\right] = \frac{1}{\alpha^2}\cos(t - \tfrac{1}{2}\pi) = \frac{\sin t}{\alpha^2}, \qquad (1.19)$$

as shown in Fig. 2(d). Thus while the forcing is proportional to $G\cos(\omega t^*)$, the response is a factor of ω smaller and is delayed by one quarter of a cycle. This represents a balance between the pressure gradient and the unsteady inertia term in (1.15). Equation (1.19) fails to satisfy the no-slip condition (1.5) at the walls; the viscous terms become important near the walls over a *boundary layer* (called a *Stokes layer*) of width (in r) of $O(1/\alpha)$, corresponding to a dimensional thickness of order $(\mu/\rho\omega)^{1/2}$, set by a balance between unsteady inertial and viscous terms in (1.15). This illustrates an important characteristic of flows for which viscous effects are weak compared to inertia ($\alpha \gg 1$, $Re \gg 1$): the flow develops thin boundary layers on solid surfaces that may play a critical role in controlling the overall flow structure.

Womersley's solution for oscillatory flow in a tube (1.18) is central to the theory of pulse propagation in arteries. We return to this below.

1.5 Almost unidirectional flows: lubrication theory

In some instances, we come across flows which are quasi-steady and almost, but not quite, unidirectional. Using Poiseuille flow as a building block (1.10), we can accurately capture the dominant physics of the problem in a very straightforward way.

For example, consider the flow along an axisymmetric tube of radius $af(Z, T)$ that varies slowly in space and time, where $z = Z/\epsilon$, f is some order-unity function and $\epsilon \ll 1$ (figure 3). Because we are thinking about flows driven by slow temporal variations of the tube's radius, we now write $t^* = T\epsilon U_0/a$, which is equivalent to replacing ω by $\epsilon U_0/a$ in (1.6) and thus α^2 by ϵRe in (1.7). The slow variation of tube radius in Z and T is accommodated by the generation of weak flows in the radial direction. We therefore set $\mathbf{u} = \epsilon v(r, Z, T)\hat{\mathbf{r}} + w(r, Z, T)\hat{\mathbf{z}}$ and $p = P(r, Z, T)/\epsilon$. We treat v, w, P, Z and T as $O(1)$ variables. The continuity equation (1.7a) becomes

$$\frac{1}{r}(rv)_r + w_Z = 0, \qquad (1.20)$$

while the axial and radial components of the momentum equation (1.7b) become

$$\epsilon Re(w_T + vw_r + ww_Z) = -P_Z + \frac{1}{r}(rw_r)_r + \epsilon^2 w_{ZZ} \qquad (1.21a)$$

$$\epsilon^3 Re(v_T + vv_r + ww_Z) = -P_r + \frac{\epsilon^2}{r}(rv_r)_r + \epsilon^4 v_{ZZ} \qquad (1.21b)$$

Assuming $\epsilon Re \ll 1$ (neglecting inertial effects relative to viscous effects), (1.21) reduces to

$$0 = -P_Z + \frac{1}{r}(rw_r)_r, \quad 0 = -P_r. \tag{1.22}$$

Thus the pressure does not vary across the tube, so that $P_Z = P_Z(Z, T)$, allowing w to be determined exactly as in Sec. 1.3. Applying the no-slip condition on $r = a$ and a boundedness condition at $r = 0$ we recover the analogue of (1.10),

$$w = -\tfrac{1}{4}P_Z(f^2 - r^2) \quad (0 \le r \le f).$$

To determine the corresponding radial flow we can use (1.20), together with the *kinematic boundary condition* that says that the radial fluid speed at the wall must match the radial wall speed,

$$v^* = (af)_{t*} \quad \text{on} \quad r^\star = af, \quad \text{i.e.} \quad v = f_T \quad \text{on} \quad r = f.$$

However rather than determine v explicity we proceed as follows. The volume flux $Q^* = a^2 U_0 Q$ satisfies

$$Q = 2\pi \int_0^f rw \, \mathrm{d}r = -\tfrac{1}{8}P_z \pi f^4,$$

so that (noting that $w = 0$ on $r = f$ and using (1.20))

$$Q_Z = 2\pi \int_0^f rw_Z \, \mathrm{d}r = -2\pi \int_0^f (rv)_r \, \mathrm{d}r = -2\pi f f_T.$$

We can write this as $(\pi f^2)_T + Q_Z = 0$. In the original dimensional variables this may be expressed as an integral statement of mass conservation $A_{t*}^* + Q_{z*}^* = 0$, where $A^* = \pi a^2 f^2$ is the tube's cross-sectional area. Thus the pressure gradient in the channel is coupled to motions of its walls by the PDE

$$(f^2)_T = \tfrac{1}{8}\left(P_Z f^4\right)_Z. \tag{1.23}$$

If the wall motion (i.e. $f(Z, T)$) is prescribed, (1.23) tells us how the internal pressure must adjust in order to enforce incompressibility. We can use (1.23) to describe *peristaltic pumping* in a tube, for example.

Alternatively, the vessel wall may be flexible, so that the pressure is a function (or a functional) of the tube area, i.e. $P = P(f)$. Then (1.23) provides an evolution equation for motion of the tube wall. We will return to this below, showing how inertial effects can be retained in the model in order to describe pulse-wave propagation, for example.

1.6 Flows in real blood vessels and airways

No artery or airway is perfectly long and straight, so the velocity profiles we have computed (parabolic Poiseuille flow, oscillatory Womersley flow or a combination of both) provide only a guide to physiological flows in most locations. In practice, bends, twists and bifurcations make real flows much more complex. While most clinicians learn about Poiseuille flow —and may base clinical decisions on it — it is rarely encountered in reality.

- *Curvature* and *torsion* induce secondary flows and distort the mean velocity profile, reducing the wall shear stress on the inside of a bend, for example. For a tube of radius a and centerline having radius of curvature R, we can define $\delta = a/R$. When $\delta \ll 1$ one can examine the leading-order effects of curvature, assuming the flow is steady and fully developed (i.e. not varying in the
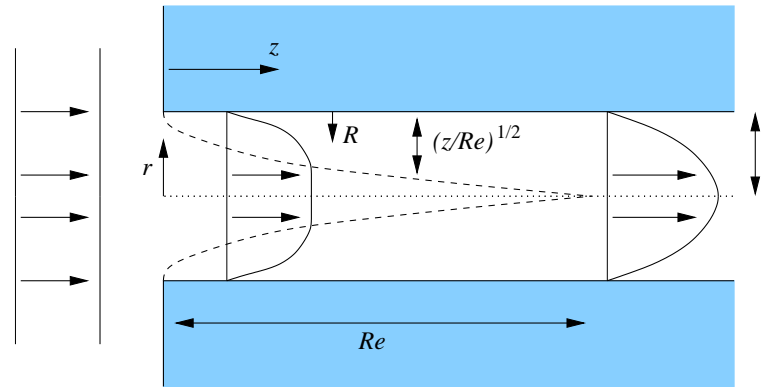
Figure 4: The development of Poiseuille flow at a tube entrance.

axial direction). The flow must experience a transverse pressure gradient (a centrifugal force) in order for the axial flow to bend with the tube. This generates a secondary flow (parameterised by the *Dean number* $\kappa = \delta^{1/2} Re$) that is coupled to the distorted axial flow. For $\kappa \ll 1$, the secondary flow has a pair of symmetric counter-rotating vortices sweeping fluid from the inside to the outside of the bend along the middle of the tube. For larger κ the secondary flow develops a complex boundary-layer structure. The nature of unsteady flows, axially varying flows, flows with large δ and flows in helical tubes remain active areas of research (see Berger, Talbot & Yao 1983).

- Sudden contractions and *expansions* (at a *stenosis*) and *branching* (at a bifurcation) induce *fbw separation*. Under steady conditions, the wall shear stress is low where the flow separates, because the flow in the eddies is relatively stagnant. This is not always the case in unsteady conditions. See Ku (1997), Berger & Jou (2000).

- After *abrupt changes* in flow direction, the flow takes a while to readjust to the uniform flows described above. When $Re \gg 1$, the adjustment arises through the formation of viscous *boundary layers*. As we shall see below, the *development length* of steady Poiseuille flow in a tube is of order aRe, so is often longer than the available distance in any straight segment of a real artery or airway.

Because high-Reynolds-number flows are extremely sensitive to the shape of the flow domain, geometric variability between individuals (and even within the same individual at different times) makes robust, reliable and accurate predictions of blood flow patterns very difficult. Models can however be used to characterise the effects of such geometric variability on blood flow patterns.

Most of these flow features require techniques that we cannot describe with the limited time available. However, we can briefly discuss how flows adjust to simple geometric changes.

1.7 Developing flows: boundary layers

We now discuss one further example illustrating the important concept of a viscous boundary layer.

Let us return to the formulation in §1.5, and suppose now that $\epsilon \ll 1$ but that $1 \ll \epsilon Re \ll \epsilon^{-2}$. We

can then retain the axial inertial term in (1.21a), so that, assuming the flow is steady, (1.20, 1.21) become

$$\frac{1}{r}(rv)_r + w_Z = 0,$$

$$\epsilon Re(vw_r + ww_Z) = -P_Z + \frac{1}{r}(rw_r)_r$$

$$0 = -P_r.$$

We can use these equations to describe the adjustment of the flow to a sudden narrowing of a tube (figure 4). Suppose, in $Z < 0$, $w = 1$ and $v = 0$, so the flow is a uniform *plug flow* in $0 \leq r \leq 1$, but that in $Z > 0$ a wall is introduced along $r = 1$ at which $w = v = 0$. The adjustment is accommodated by the viscous term, which turns out to be significant initially only near the wall. If we rescale, setting

$$r = 1 - (\epsilon Re)^{-1/2}R, \quad v = -(\epsilon Re)^{-1/2}V(R, Z), \quad w = W(Z, R),$$

then at leading order we recover

$$V_R + W_Z = 0, \quad VW_R + WW_Z = W_{RR}$$

where $V = W = 0$ on $R = 0$ and $W \to 1$ as $R \to \infty$ (to match with the plug flow in the core of the tube). We can simplify this further by setting $V = -F_Z, W = F_R$ for some function $F(R, Z)$ (called a *streamfunction*), and then the continuity equation is satisfied automatically while the momentum equation becomes

$$-F_Z F_{RR} + F_R F_{RZ} = F_{RRR},$$

with $F = F_Z = 0$ on $R = 0$ and $F_R \to 1$ as $R \to \infty$. We can transform once again, setting $R = \xi Z^{1/2}$ and assuming $F = Z^{1/2}g(\xi)$. Then the problem reduces to

$$g_{\xi\xi\xi} + \frac{1}{2}gg_{\xi\xi} = 0, \quad g(0) = g_\xi(0) = 0, \quad g_\xi \to 1 \quad \text{as} \quad \xi \to \infty.$$

This ODE has a unique solution known as the *Blasius similarity solution*. It shows us that viscous effects are confined to a boundary layer of thickness $(Z/\epsilon Re)^{1/2} = (z/Re)^{1/2}$ along the tube wall. The boundary layers merge over a distance $z = O(Re)$ along the tube, beyond which the flow is said to be fully developed.

The dissipation in Blasius boundary layers on flow dividers in bifurcations dominates the inspiratory pressure drop required to force air through multiple generations of airways (Pedley 1977).

2 Flow in collapsible tubes

Most of the vessels that carry fluids (liquids or gases) around the body are deformable. Obvious examples are veins and arteries, the ureter and urethra, the gut and lung airways. The flexibility of these vessels has a number of physiologically significant effects. We will discuss two of these effects in detail, in the context of the lung.

We first recall some basic lung physiology. The airways are arranged as a bifurcating network, with each parent airway splitting roughly symmetrically into two daughter airways at each bifurcation. In humans, there are roughly 23 generations of bifurcations from the largest airway (the trachea) down to the terminal air units (the alveoli, of which there are around 300 million in an adult lung). The lungs fit tightly inside a space confined by the rib-cage and diaphragm. On inspiration, active (muscle-driven) expansion of this space leads to expansion of the airways, which draws air into the lungs. On expiration, muscles relax and the lung typically contracts passively via its natural recoil, expelling air. Air can also be actively pushed out of the lungs (for example during the respiratory manoeuvre called *forced expiration*). Airway flexibility manifests itself in two important ways.
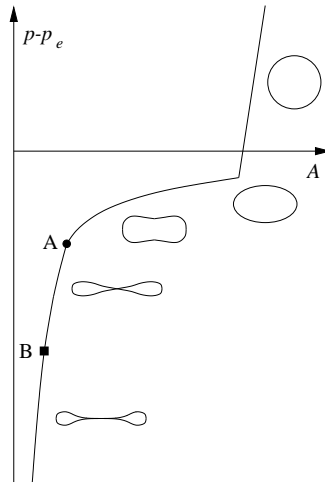
Figure 5: The relation between transmural pressure $p_{tm} = p - p_e$ and cross-sectional area α, showing typical tube cross-sections.

- *Flow limitation.* During forced expiration, active contraction of the ribs and diaphragm has two effects. First, it elevates alveolar pressure, providing a pressure gradient from alveoli to mouth that drives air out of the lungs. Second, it also elevates pressure in the tissues outside the airways. This causes the airways to partially collapse, which can inhibit expiratory flow. The net effect is that increasing the effort of expiration can, at a given lung volume, limit the maximum possible flow rate and possibly lead to a reduction in expiratory flow rate (this is known as *negative effort dependence*). Flow limitation can be a serious problem for someone having an asthmatic attack: they can have more difficulty getting CO_2 out of their lungs than getting O_2 in.

  Flow limitation is also important in the return of venous blood to the heart (particularly for giraffes!).

- *Wheezing.* One of the few non-invasive techniques for assessing lung function is to listen to the sounds generated during breathing. A forced expiration, for example, is a noisy event. Forcing air through a deformable tube can generate spontaneous oscillations of the airway walls (rather like a flag flutters in the wind), leading to audible wheezing. Other familiar sounds include those made in the upper airways during obstructive sleep apnea (snoring) and crackles associated with the popping of liquid plugs in obstructed airways.

We will now examine some simple mathematical models of the physical phenomena underlying these effects, and some of the general properties of flows through deformable tubes. (For surveys see Shapiro (1977), Kamm & Pedley (1989), Pedley & Luo (1998) and Heil & Jensen (2003).)

2.1 Deformable tubes

Consider a long elastic tube subject to variable transmural (internal minus external) pressure $p_{tm} = p - p_e$. The relationship between p_{tm} and the cross-sectional area α is shown in Fig. 5. When $p_{tm} > 0$, the tube has circular cross-section, and is under an extensional hoop stress. A tube is typically very stiff in this state (the cross-sectional area changes very little as p_{tm} increases). If p_{tm} is reduced below 0, the tube initially remains circular, but is now under compression. At a critical pressure, the tube buckles, initially to an elliptical cross-section. The compression is now balanced by bending stresses in
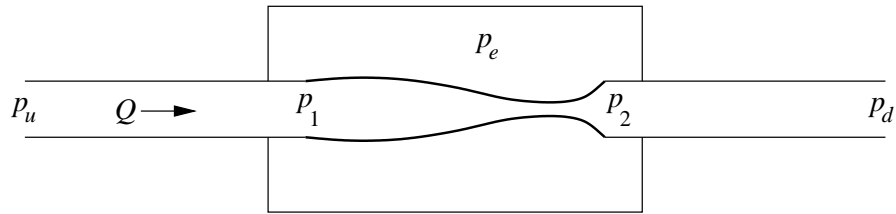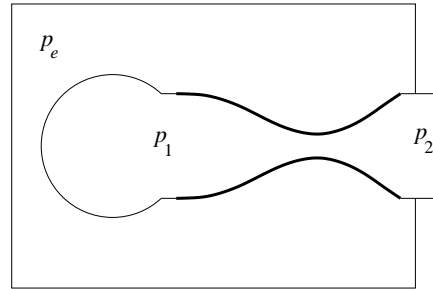
Figure 6: The Starling Resistor

Figure 7: A collapsible-tube model of the lung

the most highly curved parts of the tube wall. In this state the tube becomes highly compliant: small reductions in p_{tm} lead to large reductions in cross-sectional area. As p_{tm} is reduced further, the opposite walls of the tube come into contact first at a point, and then along a line (points A and B in Fig. 5 respectively). Thereafter, the tube forms two distinct lobes in which bending stresses are large, and further area reductions are difficult.

We have here neglected tethering, or finite length effects, which can cause the tube to buckle into more than two lobes. Lung airways, for example, which have thick, inhomogeneous walls surrounding an inextensible epithelium, can buckle into a large number of lobes.

The calculation of the tube law for an axially-uniform thin-walled elastic tube (effectively an inextensible ring that resists bending) is given using Euler–Bernoulli beam theory in Flaherty, Keller & Rubinow (1972).

2.2 The Starling Resistor

Physiologists commonly use the device shown in Fig. 6, known as the Starling Resistor, as a simple bench-top model of a deformable airway. An elastic tube is mounted between two rigid tubes, and a flow of air or water with volume flux Q is driven through the system. The experimentalist can control p_e, the pressure outside the elastic tube, and one or other of p_1 and p_2, the pressures at the upstream and downstream ends of the elastic tube, by altering the pressures at either end of the apparatus p_u and p_d.

An analogous (and crude) model for the lung is shown in Fig. 7. The intra-thoracic airways are lumped into a single compliant tube, possibly having axially varying material properties. The alveoli, which are effectively elastic-walled sacs, are represented by a balloon attached to this tube at its upstream end. p_1 corresponds to alveolar pressure, and p_e to the pleural pressure in the tissues surrounding the airways. Fixing $p_1 - p_e$ corresponds to fixing the elastic recoil of the lungs, i.e. fixing the lung volume. p_2 corresponds to atmospheric pressure at the mouth.

Simulating a forced expiration at fixed lung volume using a Starling Resistor is therefore achieved
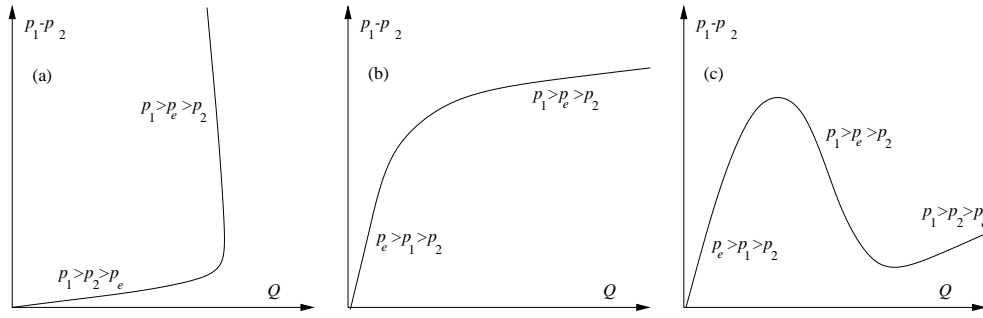
Figure 8: $p_1 - p_2$ versus Q with (a) $p_1 - p_e$ fixed, (b) $p_2 - p_e$ fixed, (c) Conrad's protocol. Time-averaged quantities are shown in cases when the flow becomes unstable.

by increasing $p_1 - p_2$, keeping the upstream transmural pressure $p_1 - p_e$ fixed. The relation between the driving pressure $p_1 - p_2$ and the steady flow Q is then as shown in Fig. 8(a). Increasing the pressure drop initially causes Q to increase: here, typically, $p_1 > p_2 > p_e$ and the tube is everywhere inflated. However, increasing $p_1 - p_2$ (for example by reducing p_2) leads to a reduction in $p_e - p_2$, which causes the tube to collapse at its downstream end (with $p_1 > p_e > p_2$). Collapse can then lead (surprisingly) to a reduction in flow-rate as $p_1 - p_2$ rises. This mimics *negative effort dependence.* Because Q cannot increase pass some threshold, this is an example of *flow limitation.*

Other protocols with the Starling Resistor also yield nonlinear pressure-drop/flow-rate relations. Increasing $p_1 - p_2$ while holding $p_2 - p_e$ constant leads to *pressure-drop limitation* (i.e. a limit on the maximum possible pressure drop, Fig. 8(b)). And in a famous experiment (Fig. 8(c)), Conrad (1969) held p_e and the downstream outlet pressure p_d fixed, as well as the resistance of a valve in the downstream rigid segment, so that p_2 increased with the flux Q according to $p_2 = kQ^2 + p_d$ for some $k > 0$. In this case,

- initially $p_e > p_1 > p_2$: the tube is collapsed along its entire length, offers a high resistance to flow, and $p_1 - p_2$ rises steeply to produce a small increase in Q; as Q increases, so do p_1 and p_2 because of the pressure drop across the valve;

- then $p_1 > p_e > p_2$: the tube inflates at its upstream end remaining collapsed downstream, the resistance to flow falls dramatically and $p_1 - p_2$ falls as Q increases;

- finally $p_1 > p_2 > p_e$: the tube is uniformly inflated, offers low resistance to flow and large increases in Q are provided by small increases in $p_1 - p_2$.

In practice, obtaining a steady pressure-drop/flow-rate curve is difficult when the flow is rapid (at large Reynolds numbers), because the Starling Resistor is prone to instabilities. Because the tube is highly compliant when it is partially collapsed (particularly when $p_1 > p_e > p_2$), small changes in the flow can lead to large changes in tube shape. The flow is strongly coupled to the shape of the wall, so shape changes lead to further flow changes. This flow-structure interaction can generate instabilities through a variety of mechanisms, that we shall explore below. Experimental measurements of the instabilities reveal a remarkably rich range of oscillations, characteristic of a complex nonlinear dynamical system.
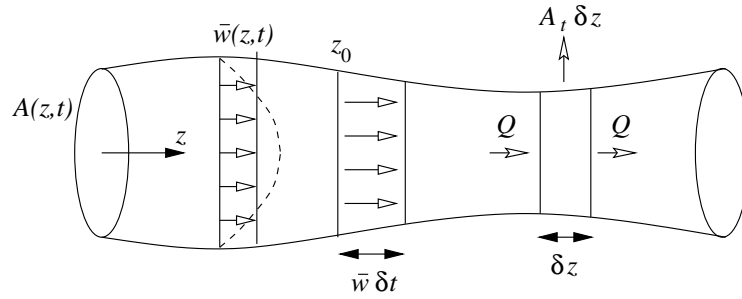
Figure 9: Mass conservation in a flexible tube.

2.3 Governing equations

While early models of flow in the Starling Resistor were based upon ODEs (describing the behavior of the system in terms of variables such as $p_1(t)$, $p_2(t)$, $Q(t)$ and $A(t)$ (the minimum area)), a more useful framework for our purposes is in terms of spatially one-dimensional models. We therefore introduce $\alpha(x,t)$, $u(x,t)$ and $p(x,t)$ as our primary dependent variables, where x measures distance along the tube and t is time. α is the tube's cross-sectional area, u the cross-sectionally averaged axial velocity and p the cross-sectionally averaged internal pressure. We need three governing equations for these three variables.

- Mass conservation: this is given by

$$\alpha_t + (u\alpha)_x = 0, \tag{2.1}$$

  where subscripts x and t denote space and time derivatives. We can understand (2.1) by considering a short section of tube, between x and $x + \delta x$, where $\delta x \ll 1$. Any difference between the volume fluxes $q = u\alpha$ entering and leaving this slice of tube must be accommodated by a change in the slice's volume, i.e.

$$(\alpha \delta x)_t = q(x, t) - q(x + \delta x, t). \tag{2.2}$$

  In the limit $\delta x \to 0$, (2.2) reduces to (2.1). This is exactly the relation we obtained in §1.5, although we are here using slightly different notation. For steady flows, the flux $q(x)$ must be uniform along the length of the tube.

- Momentum conservation: this is given by

$$\rho(u_t + uu_x) = -p_x - R(u, \alpha), \tag{2.3}$$

  where ρ is the fluid density (assumed constant) and $R > 0$ is a term representing frictional (viscous) effects. A formal derivation of (2.3) from the governing Navier–Stokes equations (1.4) is not possible in general, although we saw in Sec. 1.5 how, when the tube is axisymmetric and the flow is viscous, we can use lubrication theory for flow in a cylindrical tube to write $R \approx 8\pi\mu u/\alpha$ (compare with (1.12)).

- Pressure-area relation: this is given by
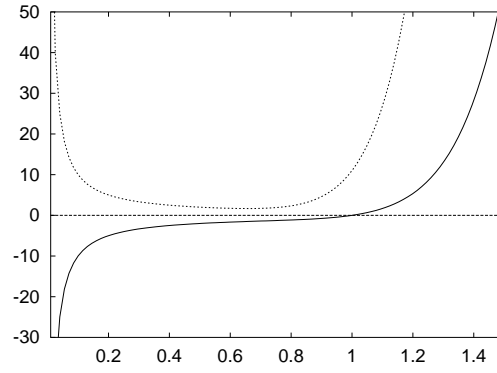
$$p - p_e = \mathcal{P}(\alpha). \tag{2.4}$$

Figure 10: $\mathcal{P}(\alpha)$ (solid) and $\alpha P'(\alpha)$ (dashed) plotted versus α, with $\mathcal{P}$ given by (2.5) with $C = 1$.

Here, $\mathcal{P}(\alpha)$ is a nonlinear function representing the static pressure-area relation for a uniform tube, such as that shown in Fig. 5. While $\mathcal{P}$ can be computed using thin-shell theory, it is simpler to use an approximate function such as

$$\mathcal{P}(\alpha) = C\left[\left(\frac{\alpha}{\alpha_0}\right)^n - \left(\frac{\alpha}{\alpha_0}\right)^{-m}\right] \tag{2.5}$$

for some constant $C > 0$, where (for example) $n = 10$ and $m = \frac{3}{2}$. This satisfies $\mathcal{P}(\alpha_0) = 0$, where α_0 is the cross-sectional area when the tube is unstressed. $\mathcal{P}(\alpha)$ and $\alpha\mathcal{P}'(\alpha)$ in this case are shown in Fig. 10: the tube is very stiff when $\alpha > \alpha_0$ or as $\alpha \to 0$, but is highly compliant (low $\mathcal{P}'(\alpha)$) in between. For small-amplitude deformations, (2.4) may be linearised, writing

$$p - p_e = K(\alpha - \alpha_0), \quad K = \mathcal{P}'(\alpha_0) > 0. \tag{2.6}$$

The quantity $1/K$ is the *compliance* of the tube (measuring the change in area for a given change in transmural pressure.) For an axially uniform, homogeneous, isotropic, thin-walled elastic tube, $K = E(h/d)/(A_0(1 - \sigma^2))$, where E is the incremental Young's modulus, h the wall thickness, $d = (4A_0/\pi)^{1/2}$ the diameter and σ Poisson's ratio. Additional terms may be added to (2.5) to represent additional physical effects: for example

$$p - p_e = \mathcal{P}(\alpha) - T\alpha_{xx} + D\alpha_t + M\alpha_{tt}. \tag{2.7}$$

Here $T \geq 0$ represents in an *ad hoc* manner the effects of longitudinal tension; α_{xx} approximates the axial component of curvature of the tube. $D \geq 0$ corresponds to viscous damping in the wall, and $M \geq 0$ accounts for wall inertia (important for air flows, because the wall-mass of a length of thin-walled tube can be comparable to the mass of the air within it).

There are important analogies between (2.1, 2.3, 2.4) and the equations of compressible gas flow in a nozzle and the equations of shallow-water flow (Shapiro 1977). Features found in these systems (such as shocks and hydraulic jumps) are manifested also in collapsible tubes.
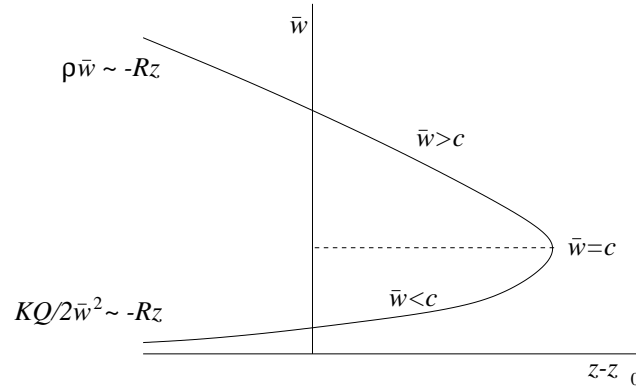
Figure 11: The solution of (2.11).

2.4 Steady flow

2.4.1 Choking

We can now explore steady flows governed by (2.1, 2.3, 2.4). For the present we take R to be a constant and set $T = M = D = 0$. Thus $q = u\alpha$ is uniform along the tube, and

$$\rho u u_x = -\mathcal{P}'(\alpha)\alpha_x - R. \tag{2.8}$$

It is convenient to define $c(\alpha)$ by

$$c = \sqrt{\alpha \mathcal{P}'(\alpha)/\rho}; \tag{2.9}$$

ρc^2 is plotted in Fig. 10. We shall see below that c is the wave-speed of small-amplitude pressure waves that can propagate along a uniform tube. We can then re-express (2.8) as

$$\rho(u^2 - c^2)u_x = -Ru. \tag{2.10}$$

We can distinguish two types of behavior. If $0 < u < c$, so-called *subcritical* flow, $u_x > 0$, implying the flow accelerates and (because $q = u\alpha$ is uniform) the tube constricts as x increases. For $u > c$, so-called *supercritical* flow, $u_x < 0$, the flow decelerates and the tube expands as x increases. The precise behavior of the tube depends on the form of the tube law. If we suppose for simplicity that c is constant (implying $\mathcal{P}(\alpha) = \rho c^2 \log(\alpha/\alpha_0)$), then we can integrate (2.10) to give

$$\tfrac{1}{2}\rho u^2 - \rho c^2 \log u = -R(x - x_0), \tag{2.11}$$

which is sketched in Fig. 11. For any initial condition, we see that the steady solution terminates at a finite value of x provided the tube is sufficiently long. This is called *choking*.

2.4.2 Non-uniform tubes

How, then, is it possible to have a steady flow in a long tube?

First, to obtain a transition from subcritical to supercritical flow we need to introduce an additional effect. In our simple lung model (Fig. 7), for example, this is provided by non-uniform material properties. Both the stiffness of the airway wall and the unstressed area α_0 may vary with position. To illustrate, assume $\mathcal{P} = K(\alpha - \alpha_0)$ where $\alpha_0 = \alpha_0(x)$ and K is constant. (We see from (2.4) that having
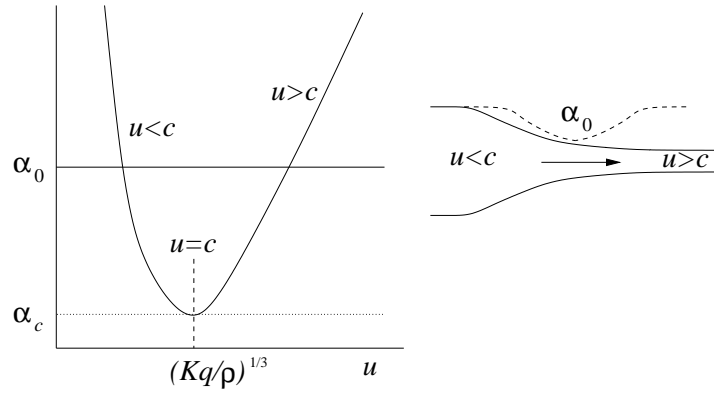
Figure 12: The graph shows how the solution of (2.14) is determined.

variable $\alpha_0(x)$ is equivalent to having variable p_e, so that we can imagine changes in α_0 being provided by a cuff placed around an otherwise uniform tube). We then have

$$\rho u u_x - \frac{Kq}{u^2} u_x = K\alpha_{0x} - R. \tag{2.12}$$

To simplify the problem, suppose $R = 0$. Now (2.12) becomes

$$\rho \frac{u_x}{u} = \frac{K\alpha_{0x}}{(u^2 - c^2)}. \tag{2.13}$$

To have a smooth transition between sub- and supercritical flow, we must have $\alpha_{0x} = 0$ where $u = c$. We can for example imagine flow through a tube with a localised constriction (so that α_0 has a local minimum, as illustrated in Fig. 12) with $0 < u < c$ upstream of the constriction and $u > c$ downstream. We can then integrate (2.12) to get

$$\tfrac{1}{2}\rho u^2 + \frac{Kq}{u} = K\alpha_0(x). \tag{2.14}$$

The solution of (2.14) is illustrated graphically in Fig. 12. Where the flow is subcritical, u increases as α_0 decreases; a smooth transition to supercritical flow can occur provided $u = c$ where $\alpha_{0x} = 0$, so $\alpha_{0\,\mathrm{min}}$ must equal

$$\alpha_c \equiv \tfrac{3}{2}(K\rho^2 q)^{1/3}, \tag{2.15}$$

the minimum value of the function on the left-hand-side of (2.14); the flow is then supercritical as α_0 rises again. If $\alpha_{0\,\mathrm{min}} > \alpha_c$ then the flow is everywhere subcritical; if $\alpha_{0\,\mathrm{min}} < \alpha_c$ there is no steady solution for these parameter values and the flow *chokes*.

Shapiro (1977) gives an exhaustive survey of such transitions.

2.4.3 Elastic Jumps

If we re-introduce friction, our supercritical solution may still terminate at finite x (as in Fig. 11), unless we can somehow return to a subcritical state. This is accommodated through an *elastic jump*. This is an abrupt transition from super- to subcritical flow, represented by a shock-like solution of the governing equations. The conditions for the transition across the jump are statements of mass and momentum
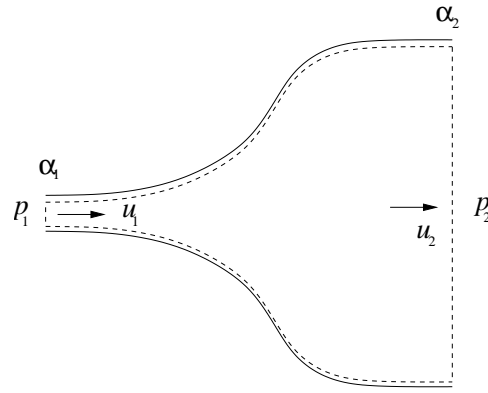
Figure 13: An elastic jump.

conservation; energy is dissipated within the jump, for example by flow separation and turbulence. Assuming the tube law can be applied throughout the jump, we have (see Fig. 13)

$$u_1 \alpha_1 = u_2 \alpha_2 \tag{2.16}$$

$$\alpha_1 (p_1 + \rho u_1^2) + \int_{\alpha_1}^{\alpha_2} \mathcal{P} \, \mathrm{d}\alpha = \alpha_2 (p_2 + \rho u_2^2). \tag{2.17}$$

Here terms of the form αp represent the horizontal force exerted by pressure on the dotted control volume. The terms $\rho \alpha u^2$ represent the momentum flux (the rate at which momentum enters and leaves the control volume).

Writing $q = u_1 \alpha_1$, the momentum condition can be re-expressed using integration by parts to give the condition that

$$\Phi = \frac{\rho q^2}{\alpha} + \int^{\alpha} a \mathcal{P}'(a) \, \mathrm{d}a \tag{2.18}$$

has equal values either side of the jump.

Using this framework, sophisticated models for flow limitation during forced expiratory flow in the lung have been developed (e.g. Elad, Kamm & Shapiro 1987). Spatial non-uniformities allow a transition from sub- to supercritical flow, and further downstream an elastic jump allows a transition from super- to subcritical flow; its position is chosen to allow the correct pressure at the mouth to be accommodated.

2.5 Unsteady flow

2.5.1 Wave propagation

Equations (2.1, 2.3, 2.7) form a closed system from which we can determine how pressure, speed and area are related during the propagation of a wave along a collapsible tube. To do so, we set $R = 0$ (ignoring viscous effects) and then linearise the governing equations, restricting attention to small-amplitude disturbances. We set

$$\alpha = \alpha_0 + \alpha_1 + \dots, \quad u = u_0 + u_1 + \dots, \quad p = p_e + p_1 + \dots,$$

where α_0, u_0 and p_e are uniform and $|\alpha_1| \ll \alpha_0$, etc. Dropping terms that are quadratic in small quantities, we have

$$\alpha_{1t} + u_0\alpha_{1x} + \alpha_0 u_{1x} = 0 \tag{2.19a}$$

$$\rho(u_{1t} + u_0 u_{1x}) = -p_{1x} \tag{2.19b}$$

$$p_1 = \mathcal{P}'(\alpha_0)\alpha_1 - T\alpha_{1xx} + D\alpha_{1t} + M\alpha_{1tt}. \tag{2.19c}$$

Writing $\mathcal{P}'(\alpha_0) = \rho c_0^2/\alpha_0$, we can eliminate p_1, and then set

$$u_1 = \Re\left(\hat{u}_1 e^{i(kx-\omega t)}\right), \quad \alpha_1 = \Re\left(\hat{\alpha}_1 e^{i(kx-\omega t)}\right)$$

for some complex amplitudes $\hat{u}_1$, $\hat{\alpha}_1$, where $\Re$ denotes 'real part.' This representation describes wave-like disturbances with wavenumber k (assumed real), wavelength $2\pi/k$, and wave crests that propagate with speed ω/k. At a fixed location, disturbances are oscillatory functions of time with angular frequency ω (if it is real) and period $2\pi/\omega$. We seek ω as a function of k. Because

$$\exp\left[i(kx - \omega t)\right] = \exp\left[i(kx - \Re(\omega)t)\right]\exp\left[\Im(\omega)t\right],$$

waves will grow or decay in time if $\Im(\omega) > 0$ or < 0 respectively.

Noting that time derivatives of u_1 and α_1 equate to multiplication by $-i\omega$ and space derivatives to multiplication by ik, (2.19) reduces to

$$\begin{pmatrix} u_0 k - \omega & k\alpha_0 \\ (kc_0^2/\alpha_0) + (Tk^3/\rho) - (i\omega Dk/\rho) - (\omega^2 Mk/\rho) & u_0 k - \omega \end{pmatrix}\begin{pmatrix} \hat{\alpha}_1 \\ \hat{u}_1 \end{pmatrix} = \begin{pmatrix} 0 \\ 0 \end{pmatrix},$$

so that a necessary condition for a solution to exist is that the matrix has zero determinant. This yields the following complex quadratic equation for ω as a function of k:

$$(u_o k - \omega)^2 - c^2 k^2 - k^4\frac{\alpha_0 T}{\rho} + i\omega\frac{Dk^2\alpha_0}{\rho} + \omega^2\frac{Mk^2\alpha_0}{\rho} = 0. \tag{2.20}$$

We can examine a number of special cases of this *dispersion relation*. When $T = D = M = 0$, we have

$$\omega = (u_0 \pm c_0)k. \tag{2.21}$$

Neutrally stable waves therefore propagate with phase speed $\omega/k = u_0 \pm c_0$. As expected, c_0 is the speed at which small-amplitude pressure waves propagate down a uniform elastic tube in the absence of a mean flow. In subcritical flow ($0 < u_0 < c_0$), waves travel upstream (with speed $c_0 - u_0$) and downstream (with speed $c_0 + u_0$). In supercritical flow ($u_0 > c_0$), all waves travel downstream. This helps us understand how flow limitation in the lung arises: if there is a region of supercritical flow, then reducing the downstream pressure need not be felt upstream because disturbances cannot propagate upstream through the region of supercritical flow. Changes may instead be accommodated by changes in the location of an elastic jump, for example.

In human arteries, $c_0 \approx 5$m/s: this is roughly the speed at which pulse waves propagate; although c_0 varies throughout out the circulation with the varying dimensions and material properties of blood vessels.

Setting $T > 0$ (with $D = M = 0$), we find that

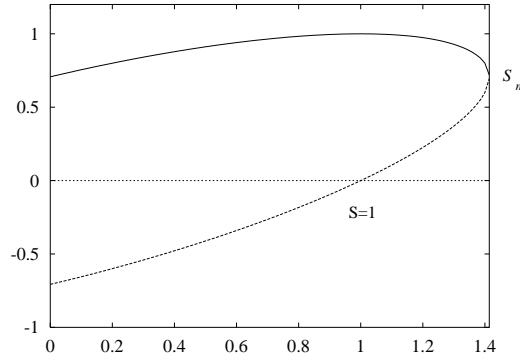$$\frac{\omega}{k} = u_0 \pm \sqrt{c_0^2 + \frac{T\alpha_0 k^2}{\rho}}. \tag{2.22}$$

Figure 14: The real part of (2.25) for $\kappa = 1$.

We see that waves of different wavelengths travel at different speeds, a phenomenon known as *dispersion*. In particular, short waves (with large k) can in principle propagate upstream through a region of supercritical flow. Tension alone is not adequate to prevent choking from occurring in some situations, however. While it must be included in distributed 1D models of flow in the Starling Resistor (Fig. 6), in order that the system is of sufficiently high order to impose boundary conditions on both pressure and height at either end of the apparatus, steady inviscid flow through this system can still choke (the tube area at some point goes to zero in finite time) if critical conditions are exceeded (Pedley 2000; Heil & Jensen 2002). This is an example of a so-called *static-divergence instability*: it has a direct explanation in terms of the Bernoulli effect: at a constriction in the tube, the speed rises (by mass conservation), the pressure falls (by Bernoulli) and so the constriction narrows further, via a direct instability.

When $D > 0$ (with $T = M = 0$), we expect that $\Im(\omega) < 0$, so that waves decay in time.

When $M > 0$ (with $T = D = 0$), then we find

$$\frac{\omega}{k} = \frac{u_0 \pm \sqrt{u_0^2 - (1 + (Mk^2\alpha_0/\rho))(u_0^2 - c_0^2)}}{1 + (Mk^2\alpha_0/\rho)}. \tag{2.23}$$

We see in this case the possibility that $\Im(\omega > 0)$, so that waves of fixed wavelength grow in time. For $0 < u_0 < c_0$ and $Mk^2\alpha_0/\rho \gg 1$ we see that there exists a root with

$$\Im(\omega) \approx \left[\frac{\rho(u_0^2 - c_0^2)}{M\alpha_0}\right]^{1/2} > 0, \tag{2.24}$$

for example. More generally, set $u_0 = Sc_0$ and $\kappa^2 = Mk^2\alpha_0/\rho$. Then

$$\frac{\omega}{c_0 k} = \frac{S \pm \sqrt{S^2 - (1 + \kappa^2)(S^2 - 1)}}{1 + \kappa^2}; \tag{2.25}$$

the real part of this quantity is plotted in Fig. 14 for $\kappa = 1$. For $0 < S < 1$, neutrally stable waves propagate both upstream and downstream, at speeds no greater than c_0 because the wall increases the overall inertia in the system. For $1 < S^2 < S_m^2 \equiv (1 + \kappa^2)/\kappa^2$, waves propagate downstream only (which may lead to flow limitation). For $S > S_m$, there exists a wave with $\Im(\omega) > 0$ which grows in time, leading to instability.

The mean flow u_0 can therefore induce *travelling wave flutter* (TWF) in a flexible tube or channel, much like a flag flaps in the wind. Surprisingly, introducing wall damping D changes this instability

to one of static divergence, in which the tube collapses through a non-oscillatory instability (Grotberg & Davis 1980). Introducing the effects of viscous dissipation in the fluid (via a term $-R = -\hat{R}u$ in (2.19b), for example) restores the oscillatory nature of the TWF instability, however (Grotberg & Reiss 1984).

TWF is a likely candidate for the generation of wheezing noises in forced expiration. It has been suggested that flutter is a signature of flow limitation, but the evidence supporting this is inconclusive (Grotberg 1994).

2.5.2 Pulse propagation

This basic theory of pulse propagation can be extended in a number of ways.

- *Reflections:* every time a wave encounters a region of spatial non-uniformity, part of the energy in the wave is transmitted through the region and part is reflected. In particular, there is wave reflection every time a pulse wave encounters an arterial bifurcation. One can use *transmission-line theory* to develop network models of wave transmission through a network of arteries.

- *Geometric attenuation:* the energy in a pulse wave is distributed through arteries of variable cross-section; as the total arterial cross section increases, the amplitude of the wave falls.

- *Dissipation:* one can use the oscillatory solutions of Sec. 1.4 to show how viscous effects cause waves to lose energy to viscous dissipation in Stokes layers.

- *Dispersion:* waves of different wavelengths and amplitudes can travel at different speeds, as in (2.22).

- *Nonlinearity:* nonlinear (finite amplitude) effects cause waves to steepen as they propagate.

Together, these effects cause the pulse-wave to change its shape significantly as it propagates along the arterial network. Changes in pulse waves can be used clinically to infer the presence of regions of vascular injury or disease.

2.5.3 Self-excited oscillations

We have seen that it is possible for steady flows to break down via choking, which reflects the non-existence of a steady flow for certain parameter values. Steady flows, if they exists, can also lose stability to oscillatory instabilities.

While TWF is a likely candidate for the generation of wheezing in lung airways, other modes of instability are observed in the Starling Resistor which could be important in both wheezing and the generation of snoring noises. For example, the Starling Resistor exhibits lower-frequency self-excited oscillations when the working fluid is water rather than air, in which case wall inertia is dominated by fluid inertia. One particular type of instability has recently been interpreted as a global mode of the whole apparatus, rather than a local mode such as we found for TWF (Heil & Jensen 2002). Much remains to be done to understand these oscillations in bench-top systems, yet more to relate them to realistic physiological conditions.

3 Surface tension effects in the lung

3.1 Surface tension and surfactants

Surface tension arises from intermolecular attractions. For molecules in the middle of a region of fluid, this attraction is isotropic. However liquid molecules near a gas/liquid interface feel a net attraction into

the liquid. A macroscopic representation of this effect is expressed by the *Young–Laplace equation*, which for fluids in equilibrium states that

$$p - p_g = \sigma \kappa \tag{3.1}$$

where p is the liquid pressure, p_g is the gas pressure, κ is the interfacial curvature and σ is the *surface tension*. An equivalent interpretation of (3.1) is that surface tension acts to reduce the area of the gas-liquid interface.

Surfactants are "surface active agents," chemicals that reduce surface tension. These are typically amphiphilic molecules such as phospholipids, having a hydrophilic head and hydrophobic tail. Insoluble surfactants form a monolayer (a monomolecular layer) at the gas-liquid interface. The hydrophilic part of the phospholipid molecule sits in the liquid, the hydrophobic part in the air. The strong attraction of the head group to nearby liquid molecules reduces the anisotropic attraction felt by liquid molecules near the interface, and hence reduces the local surface tension σ. The reduction in σ is dependent on the local surfactant concentration Γ.

3.2 Surface tension in the lung

All airways are lined with a layer of fluid. This is a sticky mucus in the larger airways, but is more watery in the smallest airways and alveoli. The tight packing of airways and alveoli in the lung means that inside the lung is an air-liquid interface of around 140m^2 (almost the size of a tennis court), most of it having very high curvature. Surface tension therefore plays an important role in lung mechanics: it contributes significantly to lung compliance (because work must be done against surface tension to inflate airways); it controls fluid balance in airways (because low capillary pressures in the liquid lining can suck liquid across permeable airway walls); and it can drive airway closure (the occlusion of flexible airway walls by the formation of liquid plugs). High surface tension is a cause of Respiratory Distress Syndrome (RDS) in premature neonates, which is characterised by stiff lungs, edema, atelectasis and poor gas exchange.

Healthy individuals maintain low levels of surface tension in the lung by producing natural *pulmonary surfactant*. This is manufactured in alveolar epithelial cells and is a complex mixture of phospholipids and proteins. At low concentrations, the reduction in surface tension σ is an approximately linear function of the local surfactant concentration Γ

$$\sigma = \sigma_0 - A\Gamma.$$

Here the constant $A > 0$ is the surfactant *activity*. At higher concentrations the $\sigma(\Gamma)$ relation becomes nonlinear.

Surfactant spreads spontaneously along airways via the *Marangoni effect*. Spatial gradients in Γ lead to gradients in σ. An interfacial gradient in surface tension drags the air-liquid interface towards the region of higher surface tension; this gradient is balanced by the viscous drag of the liquid resisting shearing of the liquid layer. Because surfactant is produced in the alveoli but not in larger airways, it is believed that surfactant spreads spontaneously proximally (mouthwards) from alveoli by this mechanism, providing a waste disposal mechanism in small unciliated airways.

An important treatment for infants with RDS due to surfactant deficiency is *Surfactant Replacement Therapy*, whereby artificial surfactant is delivered to the lung to supplement the natural supply. The subsequent reduction in surface tension makes the lung more compliant, retards airway closure and prevents pulmonary edema. Here we explore two simple flows relevant to SRT: surfactant spreading along an airway; and destabilisiation of the liquid lining of an airway by surface tension. Surveys of these and related topics are given in Grotberg (1994, 2001) and Gaver, Halpern & Jensen (2003).
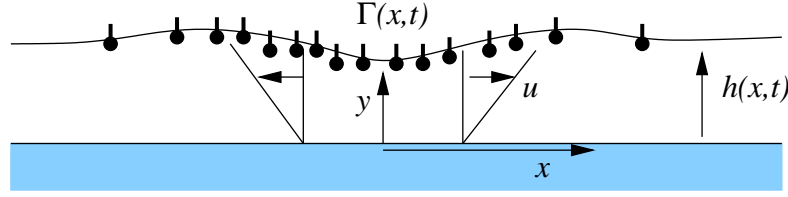
Figure 15: A surfactant monolayer on a thin liquid film.

3.3 Spreading of surfactants

A monolayer of typical concentration Γ_0 and activity A yields a surface tension reduction $S = A\Gamma_0$ (S is called the *spreading coefficient*). On a film of thickness h_0, with viscosity μ, this drives a horizontal flow of speed U_0 where

$$\frac{\mu U_0}{h_0} \sim \frac{S_0}{L_0},$$

where L_0 is the length of the monolayer. Here we have balanced the viscous shear stress (μu_y) with the surface tension gradient (σ_x); '$\sim$' denotes 'scales like.'

Now suppose $\epsilon = h_0/L_0 \ll 1$, so that we can use lubrication theory. We assume the monolayer is localized, so that the total mass of surfactant $M = \int \Gamma \, dx$ is constant during the flow. Thus $M \sim \Gamma_0 L_0$, and if $U_0 \sim L_0/t$ then

$$\frac{\mu L_0/t}{h_0} \sim \frac{AM/L_0}{L_0} \tag{3.2}$$

implying that $L_0 \sim (AMh_0t/\mu)^{1/3}$. This scaling relationship suggests that the spreading of the monolayer is *self-similar*. We will now see in detail how spreading affects the film and the surfactant distribution.

We return to the full Navier–Stokes equations (1.1, 1.4), and then simplify them using the lubrication theory reduction described in Sec. 1.5. Setting $\mathbf{u}^* = U_0(u, \epsilon v)$, $\mathbf{x}^* = L_0(x, \epsilon y)$, $p^* = (S_0/h_0)p$ and taking $Re = \rho U_0 h_0/\mu$, the governing equations are (compare 1.20, 1.21)

$$u_x + v_y = 0 \tag{3.3a}$$

$$\epsilon Re(u_t + uu_x + vu_y) = -p_x + u_{yy} + \epsilon^2 u_{xx} \tag{3.3b}$$

$$\epsilon^3 Re(v_t + uv_x + vv_y) = -p_y + \epsilon^2 y_{yy} + \epsilon^4 v_{xx} \tag{3.3c}$$

We assume this holds in $0 \leq y \leq h(x, t)$, where h is the thickness of the liquid layer (figure 15). Assuming $\epsilon Re \ll 1$, we have $0 = -p_x + u_{yy}$, $0 = -p_y$ at leading order. We impose $u = v = 0$ on $y = 0$. The layer thickness h satisfies the mass conservation equation

$$h_t + Q_x = 0, \quad Q = \int_0^h u \, dy.$$

The flow is driven by the surface tension gradient at $y = h$. When expressed in our variables, this reduces to the simple form

$$u_y = -\Gamma_x, \quad (y = h).$$

Thus the flow in the liquid layer is $u = -\Gamma_x y$, the volume flux $Q = -\Gamma_x h^2/2$ and so the film evolves according to

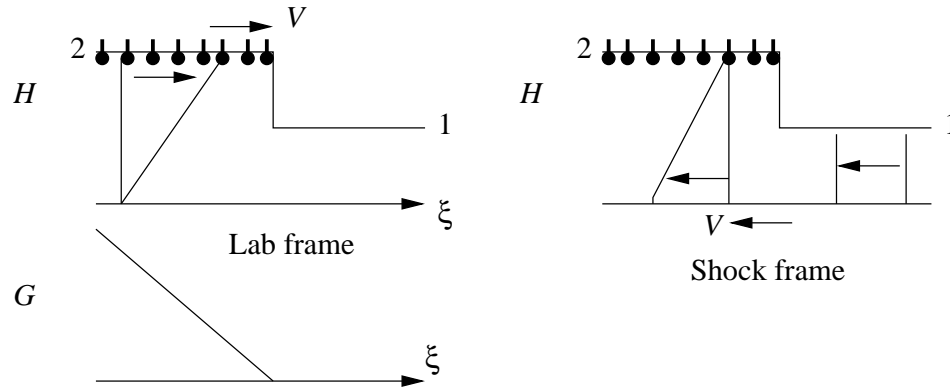$$h_t = \tfrac{1}{2} \left(h^2 \Gamma_x\right)_x. \tag{3.4a}$$

Figure 16: The kinematic shock at the leading edge of a surfactant monolayer.

To close the problem we must also account for the fact that the flow carries surfactant with it. The transport equation for surfactant at the interface is, to leading order,

$$\Gamma_t + (u_s\Gamma)_x = D\Gamma_{xx},$$

where u_s is the surface velocity and $D = D^\star/(U_0 L_0)$ is a dimensionless diffusivity. For most applications $D \ll 1$, so we may ignore this term. Thus the surfactant satisfies

$$\Gamma_t = (h\Gamma\Gamma_x)_x. \qquad (3.4b)$$

Equations (3.4a,b) provide a coupled set of evolution equations (a mixed hyperbolic/parabolic system) describing deformations to the liquid layer and the spreading of the monolayer.

3.3.1 Travelling wave solutions

We first seek travelling wave solutions of (3.4) by setting

$$h(x,t) = H(\xi), \quad \Gamma(x,t) = G(\xi), \quad \xi = x - Vt,$$

for some constant $V > 0$. Thus

$$-VH_\xi = \tfrac{1}{2}(H^2 G_\xi)_\xi, \quad -VG_\xi = (HGG_\xi)_\xi.$$

Integrating, assuming $H = 1$ and $G = 0$ for $\xi \to \infty$, gives

$$V(1 - H) = \tfrac{1}{2}H^2 G_\xi, \quad -VG = HGG_\xi,$$

so either $G = 0$ and $H = 1$ or $H = 2$ and $G_\xi = -V/2$. There is a propagating jump in film height, which is a *kinematic shock* (figure 16). In the frame of the monolayer, there is an abrupt transition between oncoming plug flow ($H = 1$, $G = 0$) and a region in which the interface is rigid ($U_s = -HG_\xi = V$), with a linear *Couette flow* underneath. Mass conservation demands that H jump from 1 to 2. Such an abrupt change violates the assumption of lubrication theory (that $\partial/\partial x^\star \ll \partial/\partial y^\star$). In practice, other effects (nonzero surfactant downstream, surface diffusion, surface tension, gravity, neglected viscous terms, inertia) become important over short lengthscales.
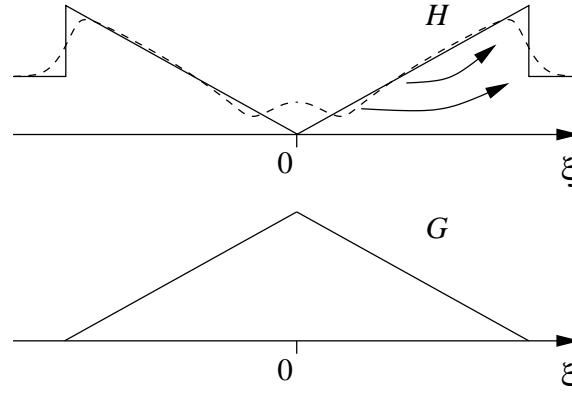
Figure 17: The dashed line sketches a solution of (3.4), the solid lines show the similarity solution (3.5), including the surface diffusion term.

3.3.2 Similarity solutions

We now seek the similarity solution of (3.4) capturing the scaling identified in (3.2) by setting

$$h(x,t) = H(\xi), \quad \Gamma(x,t) = \frac{1}{t^{1/3}}G(\xi), \quad \xi = \frac{x}{t^{1/3}}.$$

Then

$$-\tfrac{1}{3}\xi H_\xi = \tfrac{1}{2}(H^2 G_\xi)_\xi, \quad -\tfrac{1}{3}G - \tfrac{1}{3}\xi G_\xi = (HGG_\xi)_\xi.$$

We again impose $H \to 1$, $G \to 0$ as $\xi \to \infty$. Integrating, we find

$$G(HG_\xi + \tfrac{1}{3}\xi) = 0,$$

so either $G = 0$ and $H = 1$ or $HG_\xi = -\tfrac{1}{3}\xi$ and $\xi H_\xi = H$. We know from the travelling-wave solution that $H = 2$ upstream of the shock at the monolayer's leading edge, which we can set at $\xi = 1$. Thus we find $H = 1$, $G = 0$ in $\xi > 1$ and

$$H = 2\xi, \quad G = \tfrac{1}{6}(1 - \xi) \quad (0 < \xi < 1). \tag{3.5}$$

The similarity solution fails to satisfy no-flux conditions at its upstream edge, and again the shock is smoothed by other effects around $\xi = 1$, but (3.5) provides a valuable approximation to the problem that agrees well with simulations of the full PDEs (3.4), as sketched in figure 17. For further details see Jensen & Grotberg (1992).

These basic solutions underpin models of Surfactant Replacement Therapy in the lung.

3.4 Airway closure

In cylindrical polars (r, θ, z), an interface $r = R(z)$ has curvature κ $(= \nabla \cdot \mathbf{n}$, where $\mathbf{n}$ is the unit normal) given by

$$\kappa = \frac{\Delta}{R} - (\Delta R_z)_z, \quad \Delta = (1 + R_z^2)^{-1/2}. \tag{3.6}$$

Suppose a thin liquid layer lines a cylindrical tube of radius a (figure 18), with an interface at $r = R$. Put $R = a(1 - \epsilon h(x))$, where $\epsilon \ll 1$ and $z = ax$. Then the interface's curvature is

$$\kappa = \frac{1}{a}(1 + \epsilon h + \epsilon h_{xx}) + O(\epsilon^2).$$
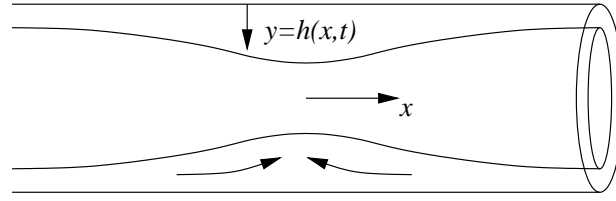
Figure 18: Surface-tension-driven flow of the liquid lining of a cylindrical tube.

Under static conditions, the pressure in the liquid lining of the tube is (from (3.1), assuming $p_g = 0$)

$$p^{\star} = -\frac{\sigma}{a}(1 + \epsilon h + \epsilon h_{xx}). \tag{3.7}$$

The term ϵh, corresponding to the azimuthal curvature of the interface, is destabilising (because an increase in film thickness increases h, lowers $p^{\star}$ and so sucks more fluid towards the thickened region, causing it to thicken further). The term ϵh_{xx}, representing the axial curvature of the interface, is stabilising. Which term wins?

Again we use lubrication theory to construct a model. With axial velocity $(\epsilon^3 \sigma/\mu)u(x, y)$ in $0 \leq y \leq h$, where $r = a(1 - \epsilon y)$, and pressure $(\epsilon \sigma/a)p(x, y)$, over times $(a\mu/\epsilon^3 \sigma)t$ the Navier–Stokes equations reduce at leading order in ϵ (once again) to

$$0 = -p_x + u_{yy}, \quad 0 = -p_y \tag{3.8}$$

with $u(x, 0) = 0$ (no slip) and $u_y(x, y) = 0$ (no shear stress, in the absence of surfactant). Integrating to find u, we obtain the volume flux $2\pi a^2 \epsilon Q$, where

$$Q = \int_0^h u \, dy = -\tfrac{1}{3}h^3 p_x.$$

The pressure (3.7) becomes $p_x = -(h + h_{xx})_x$, so that to leading order the mass conservation equation $h_t + Q_x = 0$ becomes (Hammond 1983)

$$h_t + \tfrac{1}{3}\left[h^3\left(h + h_{xx}\right)_x\right]_x = 0. \tag{3.9}$$

We can examine the linear stability of a uniform film by setting $h = 1 + h_1 e^{ikx+\omega t}$, where $h_1 \ll 1$. Linearisation of (3.9) yields the relation

$$\omega = \tfrac{1}{3}k^2(1 - k^2), \tag{3.10}$$

implying that long waves (with wavenumbers $0 < k < 1$) are unstable ($\omega > 0$), but short-wave disturbances (with $k > 1$) are stable ($\omega < 0$). So in tubes of length $L^{\star} < 2\pi a$, a thin film is stable, but for tubes that are longer than their perimeter, the thin liquid lining is likely to readjust under surface tension. For long tubes, the fastest-growing disturbance has wavenumber $k = 1/\sqrt{2}$.

Numerical simulations of (3.9) subject to periodic boundary conditions confirm this prediction, and show how the film tends to accumulate in large, isolated annular *collars*, separated by thin satellite lobes of fluid. Fluid drains slowly out of the lobes into the collars, at a rate controlled by thin transition regions at either end of the collar. As $t \to \infty$, the system approaches the quasi-static state for which $h_t \to 0$, implying $h^3(h + h_{xx})_x = 0$, for which $h = 0$ (lobes) or $h > 0$ (collars), for which h takes the form

$$h = A(1 + \cos(x - x_0)) \quad (x_0 - \pi < x < x_0 + \pi)$$

for some amplitude A and displacement x_0.

According to this thin-film model, therefore, the tube can never be blocked by its liquid lining. This is because we are assuming the film is thin (with volume $O(\epsilon a^3)$), whereas a liquid bridge requires an $O(a^3)$ volume of fluid to form. This model can be adapted to capture such behavior, by substituting the exact expression (3.6) for the curvature of the interface into (3.9). The resulting hybrid model captures accurately the rate-limiting regions of the flow (where the film is very thin and lubrication theory is applicable) as well as the large quasi-static collars, that can eventually grow large enough to form liquid bridges. For further details see Grotberg (1994).

Once a liquid bridge has formed in an airway, the low capillary pressure in the bridge places a compressive load on the airway walls. Because the walls are flexible, they can collapse under this load. The airway is then both collapsed and flooded. To reopen the airway, it must be re-inflated, which involves the propagation of a bubble of air along the airway, peeling apart wet airway walls and displacing occluding fluid until gas exchange can be restored. Theoretical models of airway reopening predict how hard one must blow to inflate a flooded, collapsed tube.

4   Blood flow in the microcirculation

Blood consists of 40-45% red blood cells (erythrocytes, RBCs) by volume, plus plasma (which is 90% water). Around 1% by volume is occupied by leukocytes, platelets, etc. The *hematocrit* H is the proportion of blood occupied by cells.

RBCs are normally biconcave disks of diameter 8μm and height 2μm. They are highly deformable, but under deformation they have roughly constant surface area (135μm^2) and volume (90μm^3). They have no nucleus; their cytoplasm is a solution of hemaglobin. The membrane is viscoelastic, with very low resistance to bending and in-plane shearing motions. It has an isotropic tension that adjusts to ensure in-plane incompressibility.

In small arterioles, capillaries and venules (of diameter under 100μm), blodd flow has negligible inertia (it is a quasi-steady Stokes flow), but blood cannot be regarded as a continuum and has highly non-Newtonian properties. In capillaries with diameters between 3 to 8μm, for example, RBCs flow in single file. An RBC cannot enter a capillary with diameter under 2.8μm.

The *apparent viscosity* μ_{app} of blood may be determined by driving flow through a tube of radius a under a pressure gradient G. If $Q^\star$ is the resulting volume flux, then by analogy with Poiseuille flow (1.11)

$$\mu_{app} = \frac{\pi a^4}{8} \frac{G}{Q^\star}.$$

The *relative viscosity* $\mu_r = \mu_{app}/\mu_0$ where μ_0 is the plasma viscosity (about 1.2 times that of water). $\mu_r \approx 4$ for whole blood in large tubes.

The *Fårhæus effect* is an observation that hematocrit H falls as the vessel diameter falls, so that H is as low as 25% in capillaries. One explanation for this is that deformable cells experience a lift away from a nearby wall, carrying them into faster moving fluid in the center of a vessel, causing cells to travel faster than the plasma (on average).

The *Fårhæus-Lindqvist effect* states that μ_r falls as diameters fall (for vessel diameters in the range 50μm to 500μm). Thus μ_r falls to around 1.3 in capillaries with diameters in the range 5-10μm. For capillaries in this range, RBCs deform significantly into a number of exotic shapes as they squeeze through the vessel. In the smallest vessels (diameter under 5μm) μ_r rises as the radius falls, since the cells reach the limit of their deformation and start to 'clog up' the vessel.

Rational models describing the motion of concentrated suspensions of deformable cells must in general be pursued computationally. However, they simplify when the cell diameter is comparable with
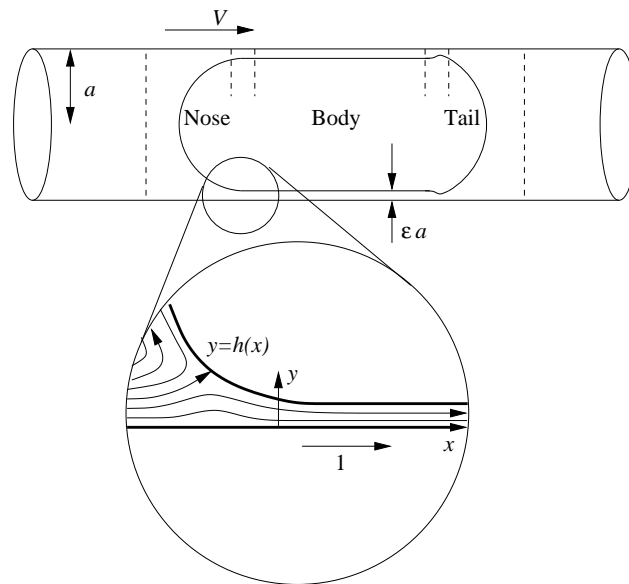
Figure 19: A red blood cell moving through a narrow capillary, drawn in the frame of the cell. The inset shows the transition region between the nose and body of the cell.

the vessel diameter, allowing cells to be treated individually. We will now examine this simple case.

4.1 Squeezing of red blood cells through narrow capillaries

We will explore a simple model for the squeezing of an RBC through a narrow tube. This is based on work in Secomb et al. (1986) and Halpern & Secomb (1989).

The cell membrane is assumed to have tension that is locally isotropic, spatially non-uniform and which ensures surface incompressibility.

We assume the cell has the shape shown in figure 19. We work in the frame of the moving cell. The large membrane tension controls the cell's shape almost everywhere. The pressure drop across the cell is given by the tension times the membrane curvature (as in the Young–Laplace equation (3.1)). Assuming viscous pressure variations are small, the pressure drop across the membrane at any point is almost uniform, and provided the tension is uniform then so is the curvature. So we can construct the shape from surfaces of uniform curvature: a hemispherical nose, a cylindrical body and a hemispherical tail. There are short transition regions (where the nose meets the body and the body meets the tail) where the membrane curvature varies abruptly, implying that the plasma pressure does also. This pressure gradient drives a viscous flow, from the body to the nose at the front of the cell and from the body to the tail at the rear. At the front transition region there is competition between the moving wall, dragging fluid into the film adjacent to the cell, and the pressure gradient pushing it out. This competition determines the thickness of the film adjacent to the cell. From this, one can determine the flux of fluid past the cell and hence the speed the cell moves relative to the average fluid speed. This in turn can be used to esimate the dependence of relative viscosity μ_r on hematocrit H for a train of cells in a capillary.

Here we seek to understand the structure of the transition region between the nose and the main body of the cell.

We know already from Section 3.4 how to use lubrication theory to approximate the flow of thin films coating tubes. Here we assume σ represents the tension in the cell membrane near the front transition region. We suppose the cell moves at speed $V^\star$ relative to the tube, and work in the frame of

the cell. We suppose the body of the cell is lubricated by a thin fluid layer of thickness ϵa, where $\epsilon \ll 1$ and a is the tube radius. In the transition region (near $z = z_t$, say), the membrane we assume lies at $R = a(1 - \epsilon h(x))$, where $z = z_t + a\epsilon^{1/2}x$. Over this short lengthscale, the leading-order expression for the pressure is (much as in (3.7))

$$p^\star = -\frac{\sigma}{a}(1 + h_{xx}). \tag{4.1}$$

The axial velocity $V^*u(x, y)$ and the pressure $(\sigma/a)p$ in the thin film ($0 \leq y \leq h$) then satisfy the lubrication-theory equations

$$0 = -p_x + (Ca/\epsilon^{3/2})u_{yy}, \quad 0 = -p_y \tag{4.2}$$

where $Ca = \mu V^\star/\sigma$ is a dimensionless parameter called the Capillary number, measuring the relative importance of viscous forces and surface tension. We seek ϵ in terms of Ca, so we assume $\epsilon = \alpha Ca^{2/3}$ for some $O(1)$ quantity α to be determined. The boundary conditions on u are $u = 1$ along $y = 0$ (no slip) and $u_y = 0$ on $y = h$ (no shear stress), implying

$$u = 1 - \tfrac{1}{2}\alpha^{3/2}p_x y(2h - y).$$

Thus the volume flux $2\pi\epsilon a^2 V^\star Q$ through the transition region is

$$Q = \int_0^h u\,\mathrm{d}y = h - \tfrac{1}{3}\alpha^{3/2}h^3 p_x \quad \text{where} \quad p_x = -h_{xxx}.$$

At the downstream end of the transition region, $h \to 1$, so that $Q \to 1$. At the upstream end, the membrane must match onto the hemispherical nose region. In the nose, the membrane has dimensional curvature $2/a$, requiring $h_{xx} \to 1$ (see (4.1)). Thus the shape of the membrane is governed by the *Landau–Levich equation*

$$1 - h = \tfrac{1}{3}\alpha^{3/2}h^3 h_{xxx}$$

with $h \to 1$ as $x \to \infty$ and $h \sim \tfrac{1}{2}x^2$ as $x \to -\infty$. Setting $x = \alpha^{1/2}3^{-1/3}\xi$, this may be written as

$$1 - h = h^3 h_{\xi\xi\xi}$$

with $h \to 1$ as $\xi \to \infty$ and $h \sim \tfrac{1}{2}\alpha 3^{-2/3}\xi^2$ as $\xi \to -\infty$. Linearising about $h = 1$, we see that there is a single eigensolution satisfying the downstream boundary condition ($h = 1 + Ae^{-\xi}$ for some constant A), implying that the problem has a unique solution (up to translation in ξ). This solution satisfies the other boundary condition for $\alpha \approx 1.337$. Thus the film thickness along the body of the cell is

$$1.337a(\mu V^*/\sigma)^{2/3}.$$

Along the side of the cell viscous forces cause the membrane tension to fall. If the cell is short, the tension is still positive at the tail, which is again hemispherical. Under certain conditions, however, the tension at the tail falls to near-zero values. The tail is then likely to assume a more highly deformed shape, possibly becoming indented.

Lubrication theory has been used to describe *tank-treading* non-axisymmetric cells, although it turns out that this motion is not kinetmatically significant. More important has been the recent discovery of *glycocalyx*, a thin polymer coating on the endothelial cells lining the interior of blood vessels. This layer, of thickness around 0.5μm, is very hard to visualise, but has a profound effect on the dynamics of tightly-fitting cells by reducing the available space for them to travel.
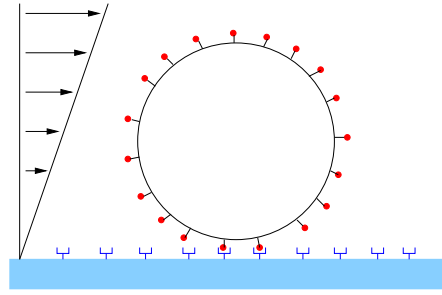
Figure 20: A cell in a shear flow rolling over an adhesive surface.

4.2   Neutrophil rolling

A further area in which lubrication finds useful application is to the adhesion of white blood cells (neutrophils, lymphocytes, etc.) to endothelial cells. Adhesion is mediated by specific receptor-ligand bonds, membrane-bound proteins that are expressed in response to stimuli as part of the inflammatory response. Adhesion is initiated through small numbers of intermolecular bonds that bind transiently, and whose binding and unbinding is strongly dependent on the mechanical forces imposed on the bonds. The whole adhesion process therefore involves interactions between thermodynamically fluctuating intermolecular bonds, deformable cell membrane, glycocalyx, and hydrodynamic forces in the suspending plasma and arising from interactions with other cells. Under suitable approximations, however, lubrication theory may be used to derive an evolution equation for the film thickness between an adherent cell and the endothelium of the form

$$h_t + Q_x = 0, \quad Q = -\tfrac{1}{12}h^3 p_x, \quad p = f(h) - h_{xx}.$$

Here $f(h)$ is a nonlinear function describing the adhesive forces of the receptor-ligand bonds, h_{xx} represents membrane tension. When solved subject to suitable boundary conditions, this evolution equation can be used to predict the rate at which a cell tank-treads over an adhesive surface when subject to an external shear flow (figure 20). For details see Hodges & Jensen (2002).

5   References

1. Berger, S.A., Talbot, L. & Yao, L.-S. (1983) Flow in curved pipes. *Ann. Rev. Fluid Mech.* **15**, 461–512.

2. Berger, S.A. & Jou, L.D. (2000) Flows in stenotic vessels. *Ann. Rev. Fluid Mech.* **32**, 347–382.

3. Conrad, W.A. (1969) Pressure-flow relationships in collapsible tubes. *IEEE Trans. Biomed. Engng* **16**, 284–295.

4. Elad, D., Kamm, R.D. & Shapiro, A.H. (1987) Choking phenomena in a lung-like model. *ASME Trans. J. Biomed. Eng.* **109**, 1–9.

5. Flaherty, J.E., Keller, J.B. & Rubinow, S.I. (1972) Post-buckling behavior of elastic tubes and rings with opoposite sides in contact. *SIAM J. Appl. Math.* **23** 446-455.

6. Gaver, D.P. III, Halpern, D. & Jensen, O.E. (2003) Surfactant and airway liquid flows. *In* 'Molecular mechanisms in lung surfactant (dys)function' in Lung Biology in Health and Disease, Marcel

Dekker Inc., New York (ed. K. Nag.) *(in press)*
Available from http://www.maths.nott.ac.uk/personal/oej/Archive/GJHchapter.pdf

7. Grotberg, J.B. (1994) Pulmonary flow and transport phenomena. *Ann. Rev. Fluid Mech.* **26**, 529-571

8. Grotberg, J.B. (2001) Respiratory Fluid Mechanics and Transport Processes. *Ann. Rev. Biomed. Eng.* **3**, 421-457.

9. Grotberg, J.B. & Davis, S.H. (1980) Fluid-dynamical flapping of a collapsible channel: sound generation and flow limitation. *J. Biomech.* **13**, 219–230.

10. Grotberg, J.B. & Reiss, E.L. (1980) Subsonic flapping flutter. *J. Sound Vib.* **92**, 349–361.

11. Hammond, P.S. (1983) Nonlinear adjustment of a thin annular film of viscous fluid surrounding a thread of another within a circular cylindrical pipe. *J. Fluid Mech.* **137**, 363–384.

12. Halpern, D. & Secomb, T.W. (1989) The squeezing of red blood cells through capillaries with near-minimal diameters. *J. Fluid Mech.* **203**, 381–400.

13. Heil, M. & Jensen, O.E. (2003) Flows in deformable tubes and channels – Theoretical models and biological applications. *In:* Flow past highly compliant boundaries and in collapsible tubes. *Eds:* T.J. Pedley and P.W. Carpenter. (Kluwer)
Available from http://www.maths.nott.ac.uk/personal/oej/Archive/heiljensenchapter.pdf

14. Hodges, S.R. & Jensen, O.E. (2002) Spreading and peeling dynamics in a model of cell adhesion. *J. Fluid Mech.* **460**, 387-409.

15. Kamm, R.D. & Pedley, T.J. (1989) Flow in collapsible tubes: a brief review, *Trans. ASME J. Biomech. Engng* **111**, 177–179.

16. Ku, D.N. (1997) Blood flow in arteries. *Ann. Rev. Fluid Mech.* **29**, 399–434.

17. Jensen, O.E. & Grotberg, J.B. (1992) Insoluble surfactant spreading on a thin viscous film: shock evolution and film rupture. *J. Fluid Mech.* **240**, 259-288.

18. Lighthill, M.J. (1975) Mathematical Biofluiddynamics. SIAM, Philadelphia.

19. McDonald, D.A. (1974) Blood flow in arteries. Camelot Press, Southampton.

20. Pedley, T.J. (1977) Pulmonary Fluid Dynamics. *Ann. Rev. Fluid Mech..* **9** 229.

21. Pedley, T.J. (1980) The fluid mechanics of large blood vessels. Cambridge University Press.

22. Pedley, T.J. (2000) Blood flow in arteries and veins. *In* Perspectives in fluid mechanics, *ed.* Batchelor, G.K., Moffatt, H.K. & Worster, M.G. Cambridge University Press.

23. Pedley, T.J. & Luo, X.Y. (1998), Modelling Flow and Oscillations in Collapsible Tubes, *Theoret. Comput. Fluid Dyn.* **10**, 277–294.

24. Secomb, T.W., Skalak, R., Oozkaya, N. & Gross, J.F. (1986) Flow of axisymmetric red blood cells in narrow capillaries. *J. Fluid Mech.* **163**, 405–423.

25. Shapiro, A.H. (1977) Steady flow in collapsible tubes. *Trans. ASME J. Biomech. Eng.* **99**, 127-147.